SEMARAK ILMU PUBLISHING

Journal of Advanced Research in Numerical Heat Transfer

Journal homepage:
https://semarakilmu.com.my/journals/index.php/arnht/index
ISSN: 2735-0142

Thermal Optimalization with CFD Analysis and Real-Time Performance Identification in Briquette Ovens Using Modbus-Based Communication

Nurul Hiron[1,*], Nundang Busaeri[1], Firmansyah Maulana Sugiartana Nursuwars[2], Aceng Sambas[3], Rachmadian Wulandana[4]

[1] Electrical Department, University of Siliwangi, Tasikmalaya, Indonesia
[2] Informatic Department, University of Siliwangi, Tasikmalaya, Indonesia
[3] Artificial Intelligence for Sustainability and Islamic Research Center (AISIR), Universiti Sultan Zainal Abidin, Campus Besut, Malaysia
[4] SUNY The State University of New York: New Paltz, NY, US

ARTICLE INFO

Article history:
Received 8 September 2024
Received in revised form 11 October 2024
Accepted 10 November 2024
Available online 15 December 2024

Keywords:
Oven; Briquette; CFD; Cradle; Modbus

ABSTRACT

Briquette ovens that utilize biomass energy frequently face obstacles in achieving consistent heat distribution, resulting in ineffective energy usage and varying product quality. This study tackles these challenges by merging Computational Fluid Dynamics (CFD) analysis, performed with Cradle software, alongside a Modbus-based temperature data acquisition system to significantly boost energy efficiency and temperature regulation. A total of 32 K-type thermocouples were meticulously positioned within the oven to gather real-time temperature data, which was processed through LabVIEW. CFD simulations revealed irregular heat distribution patterns, especially at the rear of the oven. The temperature data obtained via Modbus corroborated these observations, allowing for strategic modifications to enhance heat distribution and minimize energy loss. The system achieved an impressive accuracy rate of 98.89%, with a mere error margin of 1.11%, substantially elevating the oven's energy efficiency and briquette drying capabilities. This research clearly illustrates that the integration of CFD modeling with real-time data acquisition constitutes a powerful method for optimizing the functionality of industrial heating systems.

1. Introduction

Briquette ovens are integral to the production of coconut shell charcoal briquettes, a major export product for Indonesia, which produces over 17.1 million metric tons of coconuts annually. With the rising demand for eco-friendly fuels, especially in Europe, the Middle East, and Asia, the market for coconut briquettes is expected to grow at a CAGR of 6% by 2027. However, the production process faces challenges owing to uneven heat distribution in biomass-fueled ovens, leading to inconsistent briquette quality and inefficient energy usage. The variability of biomass fuels, such as wood, exacerbates this issue, making it difficult to maintain stable temperatures throughout the

* *Corresponding author.*
E-mail address: hiron@unsil.ac.id (Nurul Hiron)

https://doi.org/10.37934/arnht.28.1.2742

oven. This results in temperature gradients where some areas are underheated while others are overheated, causing non-uniform drying.

Nonetheless, relying solely on real-time data is insufficient to capture the intricate nature of heat dynamics in expansive ovens. Computational Fluid Dynamics (CFD) simulations provide an exceptional method for accurately modeling airflow and heat transfer. By combining CFD with real-time data acquisition, we facilitate an in-depth analysis of heat distribution, empowering us to make precise adjustments that significantly enhance energy efficiency and product quality.

Numerous studies have successfully showcased advancements aimed at enhancing the thermal efficiency of biomass ovens, especially regarding consistent heat distribution and energy optimization. Research conducted by Turhan *et al.,* [1] and Ahn [2] introduced fuzzy-based thermal control techniques that achieved an impressive 17.85% increase in energy efficiency over traditional methods. Sheng *et al.,* [3] underscored the critical need for optimizing hot air flow in biomass ovens through Computational Fluid Dynamics (CFD) analysis. Furthermore, Smolka *et al.,* [4] applied mathematical models to refine heat distribution, revealing that airflow velocity significantly influences heat uniformity in ovens. The combination of mathematical modeling and CFD for optimizing heat distribution has delivered remarkable solutions for advancing the performance of briquette ovens and biomass technology as a whole. Additionally, Sittiarttakorn and Boonto [5] utilized CFD simulations and blower systems to enhance airflow in biomass ovens. Their findings demonstrated that effective airflow management can substantially improve heat distribution uniformity in industrial drying processes. Perkasa *et al.,* [6] further reinforced the necessity of integrating fuzzy logic control systems to sustain stable temperatures in biomass ovens, significantly minimizing temperature variations, boosting energy efficiency, and elevating product quality.

Recent studies indicate that the application of nanofluids and design innovations in heat transfer systems can significantly enhance thermal efficiency. For instance, the use of Al2O3 nanofluids in shell and tube heat exchangers, as investigated by Abbood *et al.,* [7] increased heat transfer efficiency by up to 11.23%. Similarly, CNT nanofluids under laminar flow conditions exhibited an increase in Nusselt number and a reduction in skin friction factor [8]. Additionally, the use of nanoparticles such as SiO2 and TiO2 in micro-tubular heat exchangers provided high efficiency without requiring an increase in surface area [9]. In battery thermal management, Zuber *et al.,* [10] emphasized the effectiveness of Phase Change Materials (PCM) in reducing the maximum temperature of Li-ion batteries, which holds potential for electric vehicles.

In addition to innovative materials, design modifications play a critical role. Arunkumar *et al.,* [11] demonstrated that chamfered turbulators in solar air heaters can enhance thermal efficiency factors by up to 1.15. In HVAC systems, Isa *et al.,* [12] highlighted the importance of dynamic control in iris dampers to maintain indoor thermal comfort. Meanwhile, the use of corrugated twisted tape inserts in heat exchangers, as explored by Kurhade *et al.,* [13] showed significant improvements in Nusselt number. Collectively, the integration of nanofluids, PCM, and innovative designs presents substantial potential for advancing energy efficiency and thermal management across various applications.

The primary challenge presented by briquette ovens lies in their continuous operation lasting 48 hours, with temperatures meticulously set between 400C and 1000C in specific increments. Each temperature stage requires different durations to prevent thermal shock to the briquette mixture. This thermal shock can lead to inconsistent drying and ultimately compromises briquette quality.

This research is dedicated to optimizing heat distribution in coconut shell briquette ovens through the integration of real-time data acquisition and CFD validation. By enhancing energy efficiency and drying performance, this study successfully tackles operational hurdles, improves briquette quality, and lowers production costs. The overarching objective is to bolster Indonesia's standing in the global

briquette market and facilitate the widespread adoption of biomass as a viable sustainable energy alternative.

Energy management is a critical factor in the drying production process. Turbines can effectively optimize fluid flow distribution [14]. In the context of briquette ovens, capturing the thermal distribution system in real-time is vital. The significant issue arises from the extreme conditions within the oven. Thus, wireless communication systems serve as an effective solution for monitoring in such harsh environments [15], particularly in ovens operating at elevated temperatures.

1.1 Briquette Oven Technology: Current Designs and Energy Efficiency Issues

Briquette ovens have undergone remarkable improvements in energy efficiency, especially within the biomass energy domain [16]. Conventional designs continue to grapple with uneven heat distribution, resulting in variable briquette quality and heightened energy use. Research has showcased a range of methods to address these issues. For example, Obi *et al.,* [17] highlighted the necessity for superior fuel combustion and precise heat regulation, while Bhattacharya *et al.,* [19] discovered that innovations in airflow design could decrease fuel usage by 30%. Abu-Jdayil *et al.,* [20] underscored the critical role of insulation in minimizing heat loss, and Sinha *et al.,* [21] identified how fuel variability influences temperature distribution [20]. Furthermore, Aukah *et al.,* [22] illustrated the success of optimized airflow systems in enhancing drying uniformity and briquette quality.

1.2 CFD in Heat Transfer: Use of CFD Simulations for Optimizing Temperature Control

Computational Fluid Dynamics (CFD) simulations have gained immense popularity and have become an invaluable tool for thoroughly analyzing and optimizing heat transfer in a myriad of industrial processes, which prominently includes the operation of briquette ovens. The intricate details of airflow patterns, heat distribution across surfaces, and the complex temperature gradients that exist within these systems can be meticulously modeled, thus providing an opportunity to achieve significant enhancements in energy efficiency as well as ensuring the uniform drying of materials. An exemplary study conducted by [22] demonstrated that through the application of CFD technology, fuel consumption could be remarkably reduced by an impressive 15%, showcasing the practical benefits of this advanced analytical approach. Furthermore, in another insightful research effort by [16], it was shown that temperature uniformity within the systems was significantly enhanced via the optimization of airflow, while [23] illustrated the profound impact that CFD applications have on bolstering overall energy efficiency within these industrial applications. Moreover, the various heat transfer mechanisms, which include conduction, convection, and radiation, have been effectively modeled to facilitate a comprehensive analysis of the underlying heat transfer processes, as evidenced by [24]. Generally speaking, the mechanisms governing conduction heat transfer are based on Fourier's law, which describes the rate of conduction through a material as expressed in Eq. (1). In this equation, q represents the heat flux vector measured in watts per square meter (W/m²), indicating the rate at which heat is transferred across a unit area, thereby providing clarity on thermal dynamics. The variable k signifies the thermal conductivity measured in watts per meter per Kelvin (W/m·K), while the term ∇T denotes the temperature gradient vector, illustrating how temperature varies in space. Lastly, the unit vectors i, j, and k correspondingly align along the x, y, and z Cartesian coordinate directions, thus offering a complete spatial representation of the thermal behavior within the system.

$$q'' = -k\nabla T = -k\left(i\frac{\partial T}{\partial x} + j\frac{\partial T}{\partial y} + k\frac{\partial T}{\partial z}\right) \quad (1)$$

Generally, the flow of convection heat transfer uses Newton's Law of Cooling, as in Eq. (2), where the q'' is convective heat flux (W/m²), h is convective heat transfer coefficient (W/m²·K), Ts is surface temperature (K), T_∞ is fluid temperature far from the surface (K).

$$q'' = h(T_s - T_\infty) \quad (2)$$

The radiation heat transfer refers to the *Stefan-Botlzmann* law*,* as shown in Eq. (3), where the q'' is net radiative heat flux (W/m²), ϵ is emissivity of the surface (dimensionless, 0 to 1), σ is Stefan-Boltzmann constant (5.67×10^{-8} W/m²·K⁴), Ts is surface temperature (K), Tsurr is surrounding temperature (K).

$$q'' = \varepsilon\sigma(T_s^4 - T_{surr}^4) \quad (3)$$

2. Methodology

The oven was modeled based on an existing design. To capture the real-time temperature distribution, data acquisition was performed using a 32 K type thermocouple sensor with Modbus communication. The temperature data in the oven were captured in real-time at temperatures ranging from 35°C to 106°C with a data acquisition duration of 90 min. The results of this data acquisition serve as a validation of the CFD simulation.

CFD simulations were performed using the Cradle CFD (Hexagon) program. This simulation is to obtain a comprehensive picture in 2D related to the optimization of thermal distribution in the oven by considering three variations of the blower position in the oven. There are three blower positions, as shown in Figure 2. Alternative 1 is an existing condition in which the blower unit is placed above the thermal source (bimass furnace). Alternative 2 occurs when the blower unit is installed between the separators. Alternative 3 occurs when the blower unit is installed above the oven gate.

2.1 Model Oven Briquette

This study was conducted at PT. Arkelindo Bara Sejahtera, a coconut shell briquette producer in Ciamis, Indonesia. Figure 1 shows the object of study, which was a 72-cubic meter briquette oven measuring 4 × 3 × 6 meters. Figure 2 shows the hot airflow inside the oven. The oven had three main parts. Biomass furnace, oven, and separator. The biomass furnace is a hot air generator with a source of biomass, the oven is the main chamber of the oven for briquette drying, and the separator is a device used to separate hot air from the main area and inlet to the biomass furnace.

The oven was modeled based on its existing design. To capture the real-time temperature distribution, data acquisition was performed using 32 K-type thermocouple sensors with Modbus communication. Testing was conducted at temperatures ranging from 30°C to 100°C. Heat distribution optimization was attempted by placing blowers with VAWT turbines at three positions inside the oven. CFD simulations using Cradle CFD (Hexagon) were applied to analyze and optimize the blower placement.

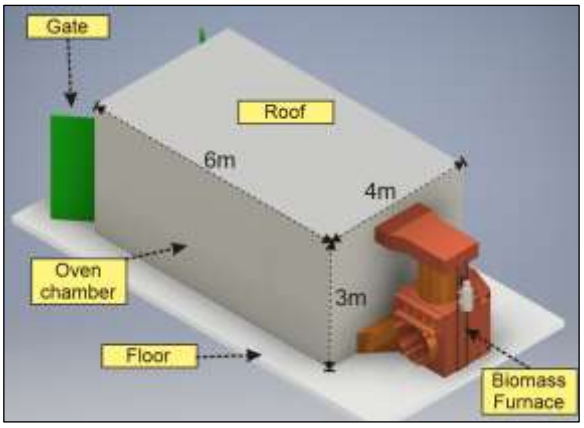

Fig. 1. 3D design of coconut charcoal oven

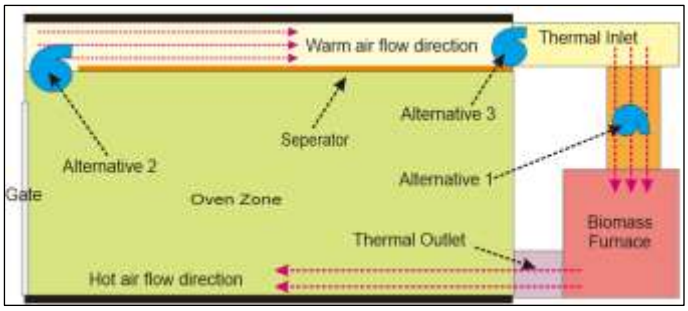

Fig. 2. Alternative variations of blower position in Briquette oven

2.2 CFD Simulation and Setup

In the simulation of thermal distribution inside a briquette oven, the method used involves the k-omega SST turbulence model. This model was chosen because of its ability to handle fluid flows involving laminar and turbulent regions simultaneously, which are commonly found in heat transfer and combustion systems. To simulate the incompressible flow of combustion gases, a virtual fan was used to model the airflow through the oven system. In addition, a no-slip boundary condition was applied to the oven wall surface to model the effect of the boundary layer on the deceleration of fluid flow around the wall. Discretization or splitting of the computational domain was performed using the hexahedral meshing method on the main area of the simulation. For areas with more complex geometries, such as parts with high curvature, polyhedral meshing is used, which is able to better follow the shape of the object. The number of elements in the simulation reached 91,000, which ensured sufficient resolution to obtain accurate results.

The simulation was run for several scenarios to observe the distribution of hot air within the oven and identify areas where heat accumulation or loss occurred. In the CFD simulation setup, a virtual fan is created at the inlet of the oven with a combustion fluid velocity of 5.5 m/s or 4.3615 m3/s.

In the CFD analysis of hot air distribution within a briquette oven, the three primary heat transfer mechanisms—conduction, convection, and radiation—are modeled using their respective equations. Conduction Eq. (1) simulates how heat moves through solid components such as the oven walls and briquettes. Convection Eq. (2) describes how heat is transferred between the hot air and the surfaces within the oven. Finally, the radiation Eq. (3) accounts for the radiative heat exchange between the surfaces and the surrounding environment. Together, these equations allow CFD simulations to accurately predict and optimize the heat distribution, ensuring efficient drying and energy usage in briquette ovens.

3. Results

3.1 Meshing

Figure 3 presents a meticulously crafted hexagonal grid meshing generated through the advanced capabilities of the Cradle Hexagon program, showcasing state-of-the-art computational modeling technology. This sophisticated grid comprises a total of 91,000 individual grid meshing elements, a deliberate choice made to ensure that computational results reflect flow dynamics and thermal distribution with exceptional detail and accuracy that mirrors real-world conditions. Given the oven's

vast dimensions, reaching an impressive volume of 72 cubic meters, it becomes crucial to employ a meshing grid featuring larger elements, as this is essential for capturing intricate temperature variations and complex airflow patterns within such a large space.

The hexagonal elements in this grid are uniformly distributed in size, significantly enhancing the simulation's ability to quantitatively detect temperature gradients and analyze air circulation patterns with high precision. This well-structured arrangement ensures that even more complex areas, including smaller compartments located on the oven's right side, are accurately represented, providing a comprehensive view of the thermal dynamics at play. The inclusion of a fine mesh in the simulation results related to thermal distribution within this large oven dimension is vital, as it allows the simulation to predict heat distribution with exceptional accuracy, a critical factor in achieving maximum drying efficiency in briquette production. This carefully designed mesh facilitates a more precise evaluation of temperature fluctuations across various volumes, especially in areas prone to significant temperature variations and where optimal air circulation is urgently needed.

Within the confines of the oven, this intricate meshing system allows for the detection of temperature changes ranging from the highest temperatures near the heat source to areas that typically exhibit cooler temperatures, such as the upper corners of the oven. Furthermore, this tightly integrated mesh plays a crucial role in analyzing airflow dynamics as it moves from the air inlet, across the main compartment, and finally exits through the hot air outlet, effectively capturing temperature gradients with high resolution that would otherwise be challenging to distinguish. Thanks to this high-resolution meshing approach, computational fluid dynamics (CFD) data provide an exceptionally detailed and comprehensive visualization of thermal distribution, which is absolutely essential for informed decision-making regarding energy efficiency and the optimization of briquette drying operations.

This advanced simulation is invaluable in its capacity to identify potential problem areas where heat may become trapped or where uneven airflow could impede the drying process, thereby offering crucial insights for improvement. In summary, this hexagonal mesh is meticulously engineered to deliver thorough numerical analysis, laying a robust foundation for enhancing thermal performance and achieving effective heat distribution within the briquette oven, ultimately paving the way for improved operational efficiency and product quality.

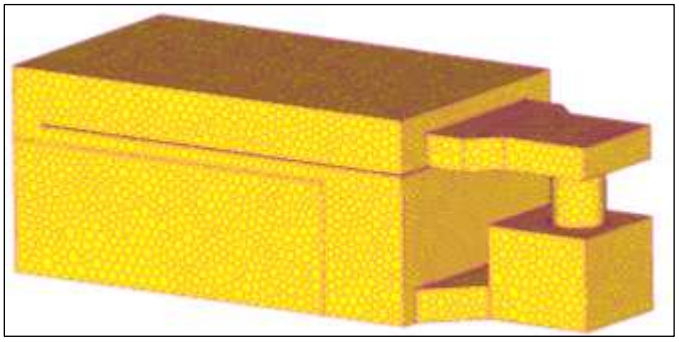

Fig. 3. Mesh computation domain

3.2 Experimental Setup

The data acquisition of the hot air flow distribution inside the briquette oven involved 32 K-type thermocouples. Thermal distribution observations are focused on two analysis perspectives: the horizontal perspective and the vertical perspective. The horizontal perspective refers to the observation of the thermal flow behavior in the horizontal area, as shown in Figure 4, and the vertical perspective refers to the observation of the thermal flow in the vertical area, as shown in Figure 5.

Thermal observations in the horizontal area were divided into four zones: 1H, 2H, 3H, and 4H. Each zone represents the thermal flow characteristics with real-time data. observations from the vertical perspective are divided into eight sections: zones 1V, 2V, 3V, 4V, 5V, 6V, 7V, and 8V as shown in Figure 5. Each measurement zone is installed with a sensor pole, where each sensor pole consists of four type-K thermocouple sensors, as shown in Figure 7. This is especially for zone 8V where thermal sensing is installed horizontally at the thermal outlet, as shown in Figure 8.

All sensors involved in the oven, both in the horizontal and vertical zones, were then connected to one Modbus module. The data cable distance from the sensors to the Modbus system was 10 m. The data communication architecture from the sensor to the Modbus protocol-based monitoring display is shown in Figure 6. The concept of data communication using Modbus allows data to be transferred over long distances with good data quality. In addition, the temperature outside the oven during data collection is quite hot, around 40^0C to 55^0C, so a sufficient distance is needed so that data collection is not interrupted.

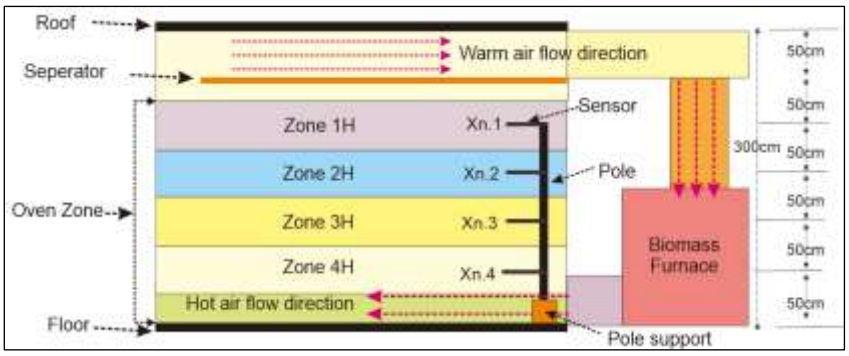

Fig. 4. Zona horizontal domain

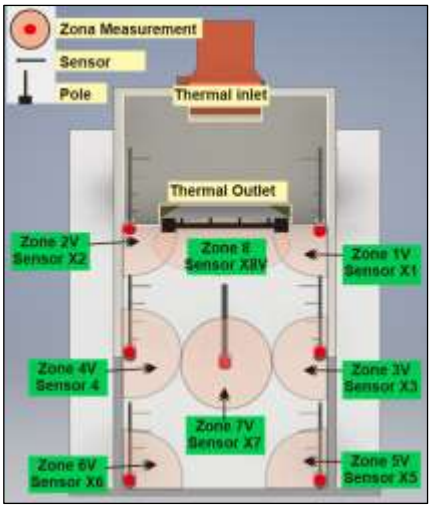

Fig. 5. Zona vertical domain

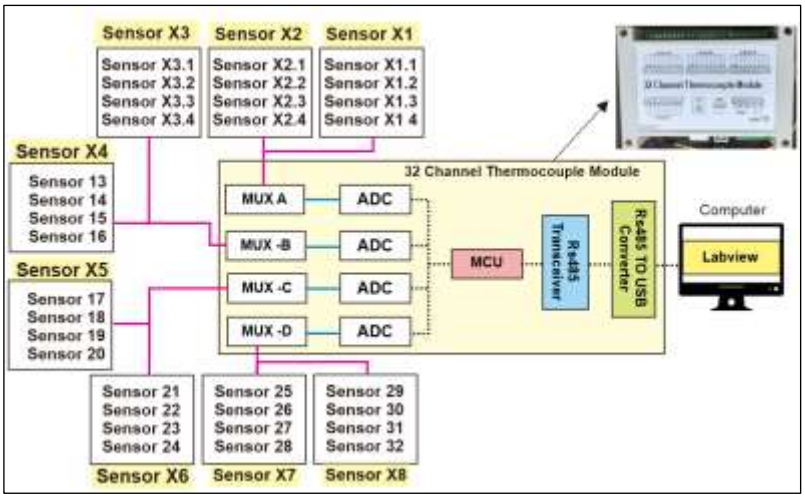

Fig. 6. Schematic of sensor modbus communication

The design of the sensor mounting position on the mast unit is shown in Figure 7. The sensor mast was designed to be positioned to stand firmly in the measurement zone. Figure 8 shows the design of the sensor mounting position on the horizontal pole. This sensor system is intended to be installed in the X8 sensor measurement zone.

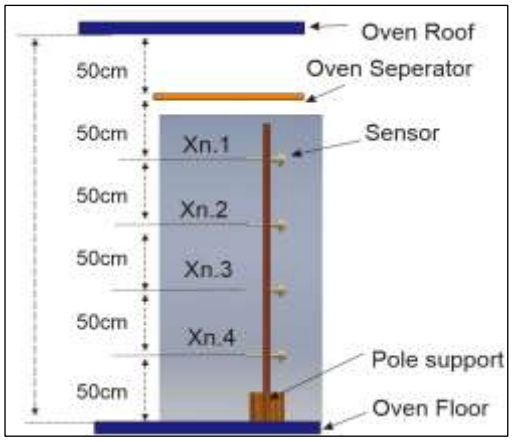

Fig. 7. Sensor formation Sensor (X1 - X7)

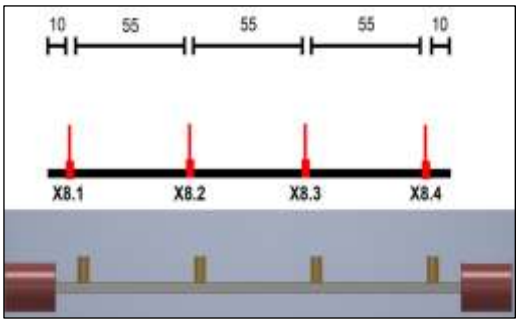

Fig. 8. Sensor formation Sensor X8

3.3 Real-Time Data Acquisition with Labview on Modbus protocol

The Modbus protocol was used to integrate the network of thermocouples with the LabVIEW software, enabling real-time data acquisition (Figure 9). This setup allowed for continuous temperature monitoring throughout the briquette drying process, providing immediate feedback on the heat distribution. The data were analyzed to identify any discrepancies between the CFD model and actual oven performance, particularly in areas where temperature inconsistencies were noted.

In configuring LabVIEW for data acquisition using 32 K-type thermocouples with the Modbus protocol, specific resource settings were applied to ensure proper communication. The baud rate was set to 9600 bps (bits per second), with eight data bits, no parity, one stop bit, and no flow control. Modbus RTU is used as the communication protocol with Master and Slave ID set to 1. The data were read through the "Read Holding Register" function, and a timeout was set at 1,000ms. This configuration allowed for smooth, real-time data acquisition from the thermocouples, ensuring accurate temperature readings across the oven.

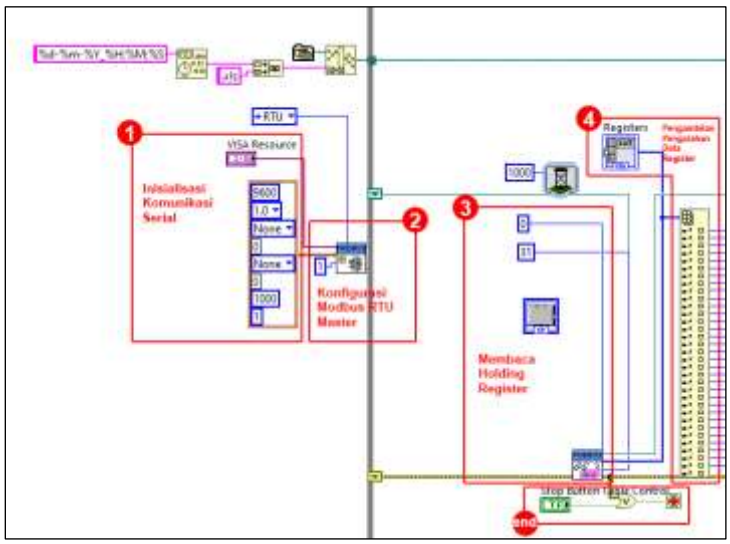

Fig. 9. Sensor data acquisition architecture with labview

The LabVIEW program in the image was divided into several key steps for Modbus communication. (1) It begins with the initialization of serial communication using the VISA Resource, where parameters such as the baud rate, parity, data bits, and stop bits are configured. (2) The

Modbus RTU Master was then set up, assigning the slave ID to identify the specific device. (3) The "Read Holding Registers" block reads data from addresses 0 to 31. (4) The retrieved data are stored in the register variable for further processing or display, and the (end) is used to terminate the communication process safely.

3.4 CFD result

The CFD simulation is displayed in 2D, which shows the thermal distribution prevailing in the oven. Vertically, observations appear to show a thermal range from 35^0C to 106^0C. Figure 10, 12, and 14 show the thermal distributions inside the oven. Figure 11, 13 and 15 show the thermal flow that occurs in the oven.

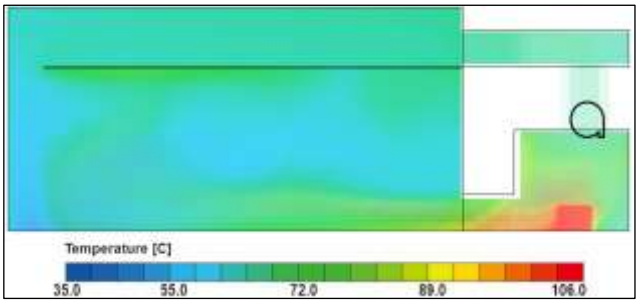

Fig. 10. Thermal distribution of alternative-1 (existing)

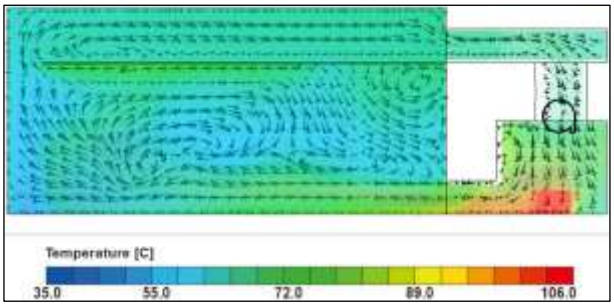

Fig. 11. Thermal direction of alternative-1 (existing)

Based on the CFD simulation results using Cradle software, Figure 10 shows uneven heat distribution in the oven under alternative-1 or existing conditions. the hotter areas (82.8°C–100°C) near the heat source and cooler zones (31°C–48.5°C) in the middle, indicating poor heat penetration. Figure 11 highlights inefficient airflow, with heat accumulating in certain regions, while other areas remain underheated, reducing overall heat uniformity. The airflow follows a path that limits the mixing of hot air, particularly in the central and upper areas, which contributes to thermal inefficiency.

The temperature distribution in the existing briquette oven, as shown by the CFD simulation, varied significantly across its dimensions. Along the length of the oven, the hottest regions (82.8°C to 100°C) are located near the heat source at the rear, while the central and front sections remain cooler, between 31.4°C and 48.5°C. In terms of height, the lower regions near the heat source exhibited high temperatures; however, as the height increased, the temperature decreased significantly, indicating inefficient vertical heat transfer. Along the width, the air distribution also remains uneven, with the sides experiencing more significant temperature gradients than the center, highlighting the need for optimized airflow to improve heat uniformity across all dimensions. This simulation result shows a lack of uniform heat distribution throughout the oven's height, resulting in uneven heating, especially at higher levels.

In Figure 12, the temperature distribution for alternative-2 shows a significant variation in heat, with lower temperature regions (15.8°C-36.8°C) occupying most of the oven's upper left section. The hottest regions (78.9°C-100°C) are concentrated near the bottom right, indicating uneven heat spread across the oven.

Figure 13 depicts the airflow pattern, which highlights the poor circulation. Hot air does not effectively reach the top-left section, leading to cooler temperatures. The airflow followed a concentrated path, resulting in heat buildup near the heat source, but insufficient heat transfer to

other areas of the oven. This demonstrates the need for improved airflow strategies to achieve a more uniform temperature distribution.

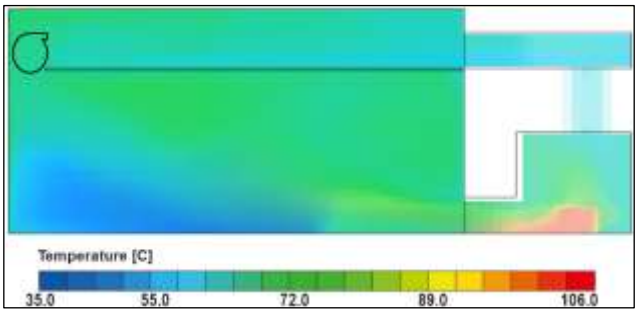

Fig. 12. Thermal distribution of alternative-2

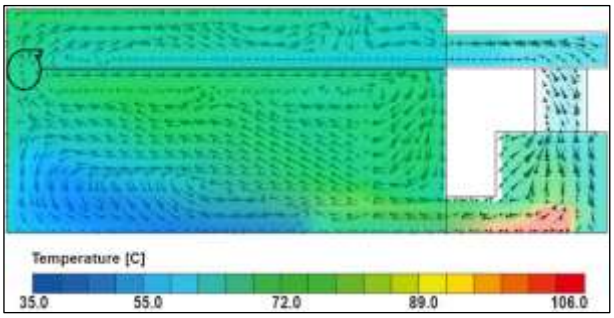

Fig. 13. Thermal direction of alternative-2

In Figure 14 (alternative-3), the temperature distribution shows that cooler regions (12.9°C-34.7°C) dominate most of the oven's interior, particularly in the upper left corner, while the hottest area (around 100°C) remains confined to the bottom-right section near the heat source.

Figure **15** illustrates the airflow direction, indicating a slightly improved circulation compared to alternative-2. However, cooler zones persist in the top-left section, and hot air is not evenly distributed throughout the oven. The airflow still failed to adequately circulate heat to all regions, indicating the need for further optimization.

Based on the CFD simulations from the three alternatives, alternative-3 (Figure 14-15) shows the most balanced airflow and temperature distribution compared to the others. Although there were still some cooler areas, the overall heat distribution was more even, particularly in the central and lower regions of the oven. The airflow direction in alternative-3 demonstrates better circulation than the existing model, providing a more consistent transfer of hot air throughout the oven. To further improve uniformity, airflow adjustments should focus on enhancing the distribution to the upper regions. Therefore, alternative-3 is the best option for achieving a more uniform heat distribution for briquette drying.

Owing to the CFD simulation, the flow from the heat source (biomass furnace) is assumed to be homogeneous with a flow velocity of 5.5 m/s or in cubication is 4.3615 m^3/s, so that other parts that are not visible in the simulation are considered the same.

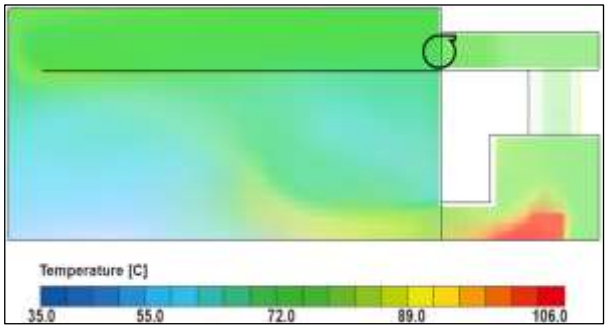

Fig. 14. Thermal distribution of alternative-3

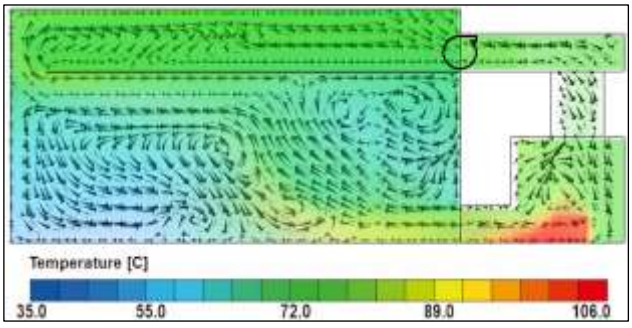

Fig. 15. Thermal direction of alternative-3

3.5 Temperature capture with sensor system

The capture of temperature inside the oven was carried out by installing eight units of sensor poles, each consisting of four sensors, as shown in Figure 7 and Figure 8. Figure 16 shows the position of the sensor unit mounted on the support pole. This configuration follows the design shown in Figure

7. Thermal data acquisition was carried out by installing the sensor pole with the formation, as shown in Figure 5, and the temperature in the biomass furnace was set within a temperature range of 40^0C-150^0C which was maintained gradually for 90 min.

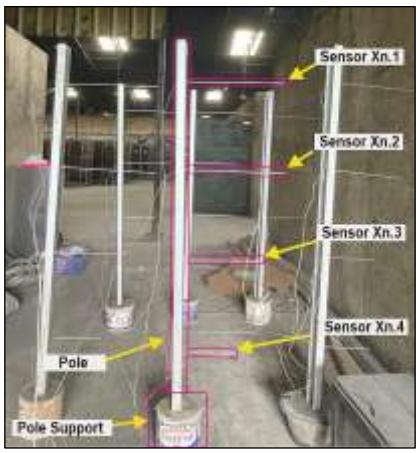

Fig. 16. Sensor configuration on the support pole

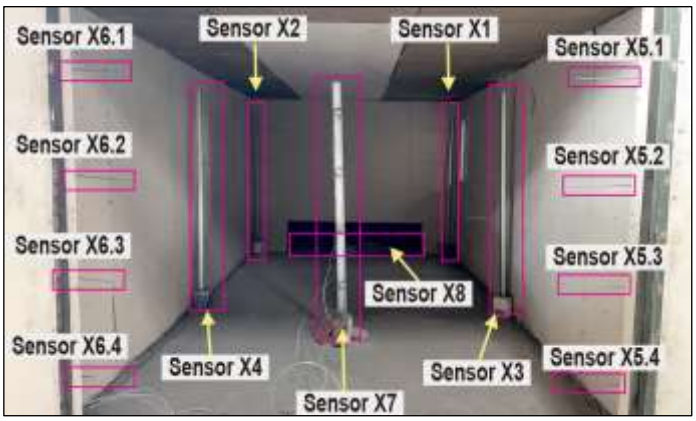

Fig. 17. Configuration of placing the sensor unit in the briquette oven

3.6 Domain zona Horizontal measurement result

Figure 18 shows the thermal capture in zone 1H or the top (see Figure 4). The results of thermal data acquisition in real-time show that the data of all sensors do not vary too much or tend to be homogeneous, with a maximum thermal temperature reaching 95^0C–103^0C. Sensor X7.1, which is located in the middle area of the upper oven, indicates a lower thermal with a maximum temperature reaching 90^0C. It can be concluded that the upper area of the oven from zone 1H, based on Figure 4, experiences a homogeneous thermal distribution except for the center.

Figure 19 shows the thermal distribution in the 2H zone area based on Figure 4. The results of thermal data acquisition show that all sensors tend to be homogeneous, with maximum thermal temperatures reaching 95^0C–100^0C. Sensor X7.2, which is located in the middle area of the oven, reaches a maximum temperature of 90^0C. These results show thermal distribution characteristics that resemble the results of the zone 1H measurements (Figure 18).

Figure 20 shows the results of the data acquisition in zone 3H. The thermal distribution data tended to be inhomogeneous. Sensor X4.3 shows the highest temperature reaching 106^0C, while sensor X7.3 shows the lowest temperature reaching 90^0C. and sensor X1.3, sensor X2.3, sensor X3.3, sensor X5.3, and sensor X6.3 show the same temperature that tends to reach 95^0C maximum. These results indicate that the thermal distribution in zone 3H has characteristics in which high temperatures tend to be dominant on the right wall of the oven (sensor X.4.3). and low temperatures tended to be dominant in the middle area (sensor X7.3), and the rest were homogeneously at 95^0C.

Figure 21 shows the capture of the thermal distribution at the bottom or zone 4H. It appears that the high temperature is dominant in sensor X8, located at the thermal outlet (see Figure 5), with temperatures reaching 110^0C. while the temperature in the biomass furnace reaches 120^0C, meaning that there is a thermal loss of 30^0C wasted in the furnace and tunnel area. High temperatures are also dominant in sensor X4.4 which reaches 105^0C. Temperature variations between 98^0C to 80^0C are scattered on other sensors.

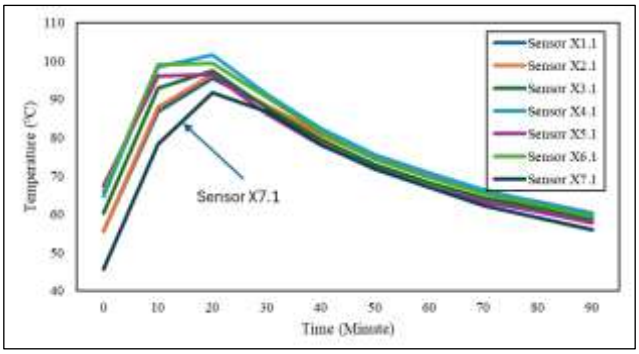

Fig. 18. Temperature capture on zone 1H

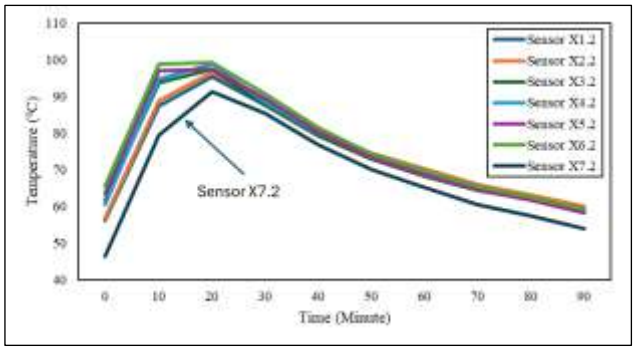

Fig. 19. Temperature capture on zone 2H

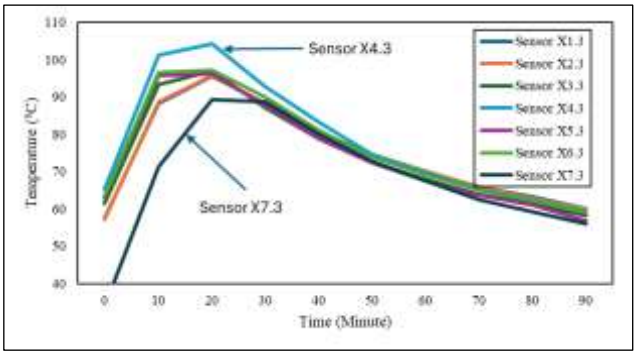

Fig. 20. Temperature capture on zone 3H

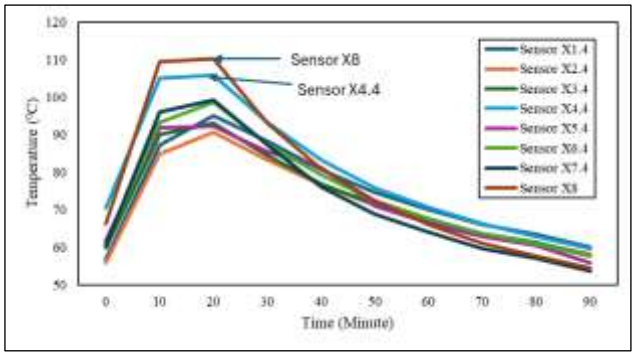

Fig. 21. Temperature capture on zone 4H

The results of thermal temperature data acquisition in the oven show that the upper area in the oven chamber (zones 1H and 2H) has a homogeneous temperature, although the middle part has a lower temperature. Low temperatures were also dominant in the lower area of the oven chamber (Zones 3H and zone 4H). The highest temperature was detected at sensor X8, which was exposed at the thermal outlet. From all real-time data acquisition experiments with a duration of 90 minutes and a thermal flow rate of 5.5m/s, it appears that the maximum thermal temperature is reached from 10 minutes to 20 minutes.

3.7 Domain Zona Vertikal Measurement Result

The analysis of Figures 22-29 reveals the vertical distribution of hot air flow in each zone from 1V to zone 8V acquired by sensor units X1 to X8. The temperature levels are separated by height with a distance of 50 cm, as shown in Figure 7. The results of this data acquisition were an observation of the thermal distribution performance from a vertical perspective.

Figure 22 shows the temperature capture in zone 1V by sensor X1. It appears that the temperature around the pole of sensor X1 is homogeneous. The average temperature is 74.12^{0}C, and the maximum temperature reaches 95.3^{0}C at 20 minutes. While Figure 23 shows the temperature capture from sensor X2, it appears to show a homogeneous temperature at the top (sensor X2.1-sensor X.2.3), whereas the temperature at 50 cm (sensor X2.4) above the floor appears lower. The average temperature at sensor X2 is 73.6^{0}C and the maximum temperature reaches 94.8^{0}C at 10 to 20 minutes.

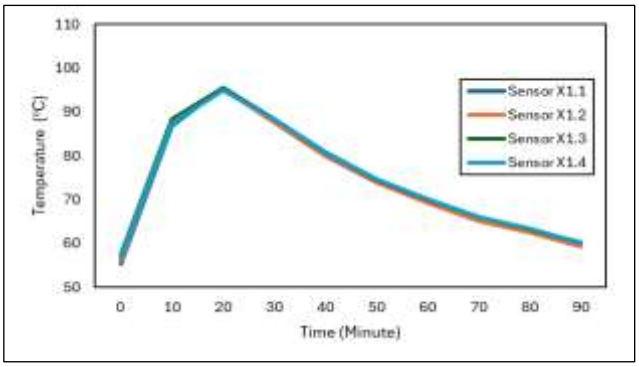

Fig. 22. Temperature capture on zone 1V (sensor X1)

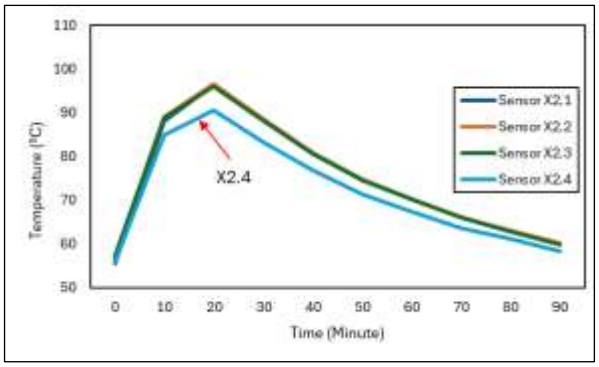

Fig. 23. Temperature capture on zone 2V (sensor X2)

Figure 24 shows the temperature capture at zone 3V by sensor X3. It appears that the temperature behaves homogeneously at all sensors, but at sensor X3.4, it is lower. This result indicated that the temperature at the bottom of the oven tended to be lower. The average temperature is 73.9^{0}C and the maximum temperature is 96.2^{0}C. Figure 25 shows the temperature capture in zone 4V by sensor X4. It appears that the thermal distribution is not homogeneous, with insignificant variations. The average temperature is 77.5^{0}C and the maximum temperature is 102.7^{0}C.

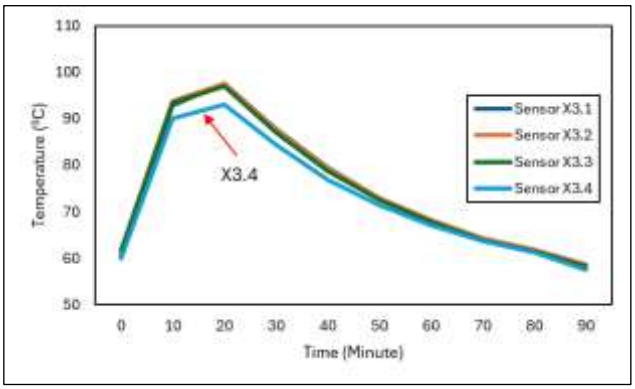

Fig. 24. Temperature capture on zone 3V (sensor X3)

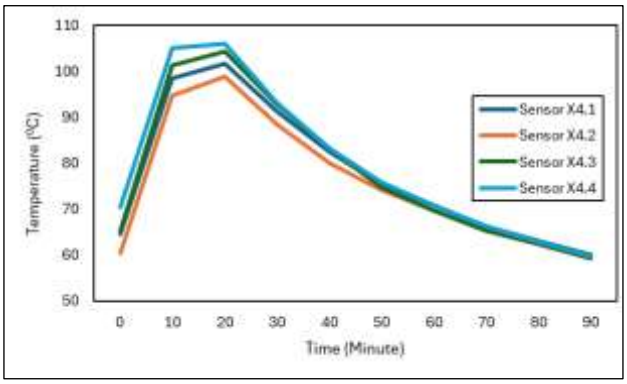

Fig. 25. Temperature capture on zone 4V (sensor X4)

Figure 26 shows the thermal temperature capture at zone 5V from sensor X5. The average temperature detected was 74.3^{0}C, while the maximum temperature reached 95.6^{0}C. it appears that the four sensors (X5.1, X5.2, X5.3) show homogeneous data around 98^{0}C, while sensor X5.4 shows a lower temperature value of 90^{0}C. It can be concluded that the capture temperature at the bottom was lower than that at the top.

Figure 27 shows the temperature capture in zone 6V by sensor X6. It appears that the thermal distribution tends to be homogeneous with insignificant variations. The average temperature is 75.9^{0}C and the maximum temperature reaches 98.6^{0}C. It is concluded that in zone 6V, there is a homogeneous thermal distribution.

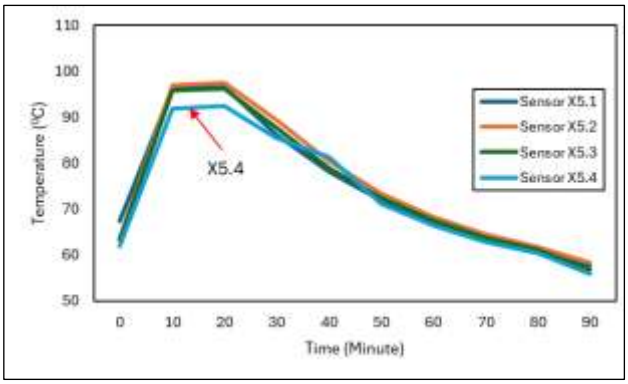

Fig. 26. Temperature capture on zone 5V (sensor X5)

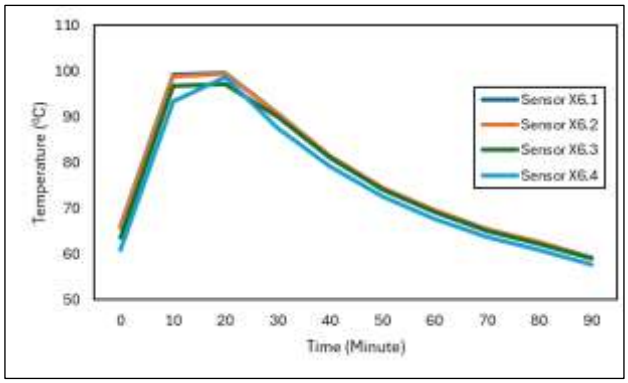

Fig. 27. Temperature capture on zone 6V (sensor X6)

Figure 28 shows a varied thermal distribution. It appears that sensor X7.4 has the highest temperature, reaching 100^0C. while sensors X7.2, X7.3, and sensor X7.3 seem homogeneous. The average thermal temperature is 69.7^0C, and the maximum temperature reaches 92^0C. This means that the temperature at the bottom of sensor X7 was higher than that of the top sensor.

Figure 29 shows high and homogeneous temperature data for sensors X8.2, X8.3, and X8.4, reaching a maximum temperature of 115^0C, while sensor X8.1 shows a lower temperature, reaching 100^0C. The position of sensor X8.1 is on the right (Figure 8).

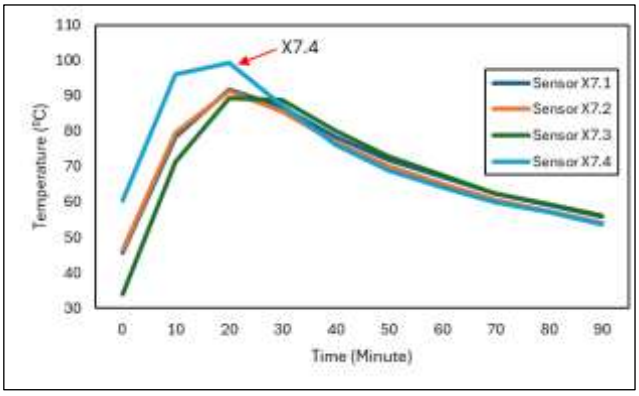

Fig. 28. Temperature capture on zone 7 (sensor X7)

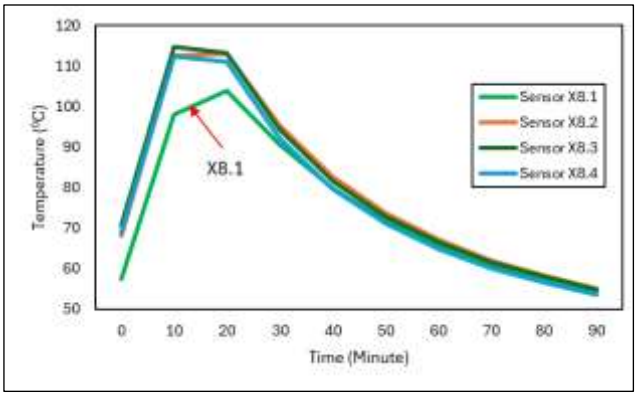

Fig. 29. Temperature capture on zone 8 (sensor X8)

In Figures 28 and 29, the data show that Sensor X7, located in the center of the oven, exhibits a more balanced temperature profile compared to sensors positioned on the walls. This indicates that the middle of the oven experienced a more stable and averaged temperature. On the other hand, Sensor X8, placed at the hot-air outlet, captures temperatures indicating the heat leaving the oven. The consistent readings from Sensor X8 suggest that the heat is being efficiently evacuated, although the overall distribution inside the oven remains uneven.

The analysis of Figures 22-29 reveals that the oven's thermal distribution system is not functioning optimally, especially in the center area. Sensors on the right side consistently recorded higher temperatures than those on the left side, indicating uneven heat distribution across the oven. Additionally, the vertical heat distribution shows temperature variations, with higher temperatures near the bottom. The central sensor (X7) reflects relatively balanced conditions, but overall, the system needs improvements, particularly in airflow control on the left side and at higher levels, to achieve a uniform temperature distribution and efficient briquette drying.

4. Conclusions

The study results that the ovens with existing designs show uneven thermal distribution, which causes poor oven performance. Real-time measurement result indicates that the thermal distribution within the oven is more homogeneous on the left wall (sensor X1, sensor X3, and sensor X5) than on the right wall (sensor X2, sensor X4, and sensor X6). The middle part was found to have a lower temperature (sensor X7). Horizontally, the upper sections of the oven showed better heat uniformity than the lower sections. Data acquisition using the Modbus protocol and 32 thermocouple sensors successfully captured detailed and accurate temperature readings. The CFD analysis provided comprehensive insights into both the heat distribution and airflow direction. Both real-time data acquisition and CFD simulations aligned well, with alternative 4 emerging as the best design, offering the most uniform thermal distribution, particularly in the 35^0–106°C range. Of the three alternative blower placement proposals, the CFD simulation results show that alternative 3 shows a more even thermal distribution than alternative 1 or alternative 2.

References

[1] Turhan, Cihan, Silvio Simani, and Gulden Gokcen Akkurt. "Development of a personalized thermal comfort driven controller for HVAC systems." *Energy* 237 (2021): 121568. https://doi.org/10.1016/j.energy.2021.121568

[2] Ahn, Jonghoon. "Performance analyses of temperature controls by a network-based learning controller for an indoor space in a cold area." *Sustainability* 12, no. 20 (2020): 8515. https://doi.org/10.3390/su12208515

[3] Sheng, Tuo, Haifeng Luo, and Mingliang Wu. "Design and Simulation of a Multi-Channel Biomass Hot Air Furnace with an Intelligent Temperature Control System." *Agriculture* 14, no. 3 (2024): 419. https://doi.org/10.3390/agriculture14030419

[4] Smolka, Jacek, Zbigniew Bulinski, and Andrzej J. Nowak. "The experimental validation of a CFD model for a heating oven with natural air circulation." *Applied thermal engineering* 54, no. 2 (2013): 387-398. https://doi.org/10.1016/j.applthermaleng.2013.02.014

[5] Sittiarttakorn, Vuttichai, and Sudchai Boonto. "Temperature control and stabilization of an industrial oven using thermoelectric devices as the stabilize actuator." *Journal of the Japan Society of Applied Electromagnetics and Mechanics* 27, no. 3 (2019): 366-370.

[6] Perkasa, Imam Wahyu Putra, Fachrudin Hunaini, and Sabar Setiawidayat. "Protoype Burner Control of Gas Fuel Oven Machine using Fuzzy Logic Control and Wireless Data Monitoring." *JEEE-U (Journal of Electrical and Electronic Engineering-UMSIDA)* 5, no. 1 (2021): 1-21. https://doi.org/10.21070/jeeeu.v5i1.1005

[7] Abbood, Mohammed, Yaser Alaiwi, and Ahmad Jundi. "Numerical Analysis and Design for Thermal Efficiency Optimization using Al2O3 Nanofluids in Shell and Tube Heat Exchangers." *CFD Letters* 16, no. 11 (2024): 146-160. https://doi.org/10.37934/cfdl.16.11.146160

[8] Awad, Afrah Turki, Abdulelah Hameed Yaseen, and Adnan M. Hussein. "Evaluation of Heat Transfer and Fluid Dynamics across a Backward Facing Step for Mobile Cooling Applications Utilizing CNT Nanofluid in Laminar Conditions." *CFD Letters* 16, no. 10 (2024): 140-153. https://doi.org/10.37934/cfdl.16.10.140153

[9] Bennoud, Salim, and Merouane Salhi. "Heat Transfer Improvement by Exploitation of Nanofluids in a Tubular Heat Exchanger." *Journal of Advanced Research in Fluid Mechanics and Thermal Sciences* 120, no. 2 (2024): 137-154. https://doi.org/10.37934/arfmts.120.2.137154

[10] Zuber, Mohammad, K. N. Chethan, Laxmikant G. Keni, Irfan Anjum Badruddin Magami, and Chandrakant R. Kini. "Enhancing Electric Vehicle Battery Thermal Management using Phase Change Materials: A CFD Analysis for Improved Heat Dissipation." *CFD Letters* 16, no. 8 (2024): 138-149. https://doi.org/10.37934/cfdl.16.8.138149

[11] Arunkumar, H. S., N. Madhwesh, Anirudh Hegde, Manjunath Mallashetty Shivamallaiah, Kota Vasudeva Karanth, and Younes Amini. "Effect of chamfered turbulators on performance of solar air heater-numerical study." *CFD Letters* 16, no. 11 (2024): 17-36. https://doi.org/10.37934/cfdl.16.11.1736

[12] Isa, Norasikin Mat, Azian Hariri, Mohamed Hussein, and David Shina Adebayo. "Exploring the Effect of Indoor Thermal Comfort using Iris Dampers: A Justification Study." *Journal of Advanced Research in Fluid Mechanics and Thermal Sciences* 121, no. 2 (2024): 1-11. https://doi.org/10.37934/arfmts.121.2.111

[13] Kurhade, Anant Sidhappa, Govindarajan Murali, Pallavi Abhinandan Jadhav, Parimal Sharad Bhambare, Shital Yashwant Waware, Tushar Gadekar, Rahul Shivaji Yadav, Ramdas Biradar, and Prashant Patil. "Performance Analysis of Corrugated Twisted Tape Inserts for Heat Transfer Augmentation." *Journal of Advanced Research in Fluid Mechanics and Thermal Sciences* 121, no. 2 (2024): 192-200. https://doi.org/10.37934/arfmts.121.2.192200

[14] Hiron, Nurul, Ida Ayu Dwi Giriantari, Lie Jasa, and I. Nyoman Satya Kumara. "The Performance of a Three-blades Fish-ridge Turbine in an Oscillating Water Column System for Low Waves." In *2019 International Conference on Sustainable Engineering and Creative Computing (ICSECC)*, pp. 30-35. IEEE, 2019. https://doi.org/10.1109/ICSECC.2019.8907013

[15] Hiron, Nurul, Asep Andang, and Nundang Busaeri. "Investigation of Wireless Communication from Under Seawater to Open Air with Xbee Pro S2B Based on IEEE 802.15. 4 (Case Study: West Java Pangandaran Offshore Indonesia)." In *Proceedings of the Future Technologies Conference (FTC) 2018: Volume 2*, pp. 672-681. Springer International Publishing, 2019. https://doi.org/10.1007/978-3-030-02683-7_47

[16] Abbood, Mohammed, Yaser Alaiwi, and Ahmad Jundi. "Numerical Analysis and Design for Thermal Efficiency Optimization using Al2O3 Nanofluids in Shell and Tube Heat Exchangers." *CFD Letters* 16, no. 11 (2024): 146-160. https://doi.org/10.37934/cfdl.16.11.146160

[17] Obi, Okey Francis, Ralf Pecenka, and Michael J. Clifford. "A review of biomass briquette binders and quality parameters." *Energies* 15, no. 7 (2022): 2426. https://doi.org/10.3390/en15072426

[18] Shaisundaram, V. S., M. Chandrasekaran, S. Sujith, KJ Praveen Kumar, and Mohanraj Shanmugam. "Design and analysis of novel biomass stove." *Materials Today: Proceedings* 46 (2021): 4054-4058. https://doi.org/10.1016/j.matpr.2021.02.569

[19] Bhattacharya, S. C., M. Augustus Leon, and Md Mizanur Rahman. "A study on improved biomass briquetting." *Energy for sustainable development* 6, no. 2 (2002): 67-71. https://doi.org/10.1016/S0973-0826(08)60317-8

[20] Abu-Jdayil, Basim, Abdel-Hamid Mourad, Waseem Hittini, Muzamil Hassan, and Suhaib Hameedi. "Traditional, state-of-the-art and renewable thermal building insulation materials: An overview." *Construction and Building Materials* 214 (2019): 709-735. https://doi.org/10.1016/j.conbuildmat.2019.04.102

[21] Sinha, Rahul, Bathina Chaitanya, Birendra Kumar Rajan, Anurag Agarwal, Ajay D. Thakur, and Rishi Raj. "Design, fabrication, and performance evaluation of a novel biomass-gasification-based hot water generation system." *Energy* 185 (2019): 148-157. https://doi.org/10.1016/j.energy.2019.06.186

[22] Aukah, Jackis, Mutuku Muvengei, Hiram Ndiritu, and Calvin Onyango. "Optimization of the performance of hybrid solar biomass dryer for drying Maize using ANSYS workbench." *Journal of Energy Research and Reviews* 4, no. 1 (2020): 50-69. https://doi.org/10.9734/jenrr/2020/v4i130119

[23] Anand, Sumeet, Dipti Prasad Mishra, and Shailesh Kumar Sarangi. "CFD supported performance analysis of an innovative biomass dryer." *Renewable Energy* 159 (2020): 860-872. https://doi.org/10.1016/j.renene.2020.06.039

[24] Chilka, Amarvir G., and Vivek V. Ranade. "CFD modelling of almond drying in a tray dryer." *The Canadian Journal of Chemical Engineering* 97, no. 2 (2019): 560-572. https://doi.org/10.1002/cjce.23357

[25] Al Qubeissi, Mansour. "Developing a conjugate heat transfer solver." *International Journal of Mathematical, Computational, Physical, Electrical and Computer Engineering* 6, no. 7 (2012): 782-787.